

Photonic crystal nanocavity based on a topological corner state: supplementary material

YASUTOMO OTA^{1*}, FENG LIU², RYOTA KATSUMI³, KATSUYUKI WATANABE¹,
KATSUNORI WAKABAYASHI^{2,4}, YASUHIKO ARAKAWA¹ AND SATOSHI IWAMOTO^{1,3}

¹Institute for Nano Quantum Information Electronics, The University of Tokyo, 4-6-1 Komaba, Meguro-ku, Tokyo, 153-8505 Japan

²Department of Nanotechnology for Sustainable Energy, School of Science and Technology, Kwansai Gakuin University, Gakuen 2-1, Sanda 669-1337, Japan

³Institute of Industrial Science, The University of Tokyo, 4-6-1 Komaba, Meguro-ku, Tokyo, 153-8505 Japan

⁴National Institute for Materials Science, Namiki 1-1, Tsukuba 305-0044, Japan

*Corresponding author: ota@iis.u-tokyo.ac.jp

Published 31 May 2019

This document provides supplementary information to “Photonic crystal nanocavity based on a topological corner state,” <https://doi.org/10.1364/OPTICA.6.000786>.

1. Zak phase and the emergence of the topological corner state

The topological corner states discussed in the main text originate from the nontrivial Zak phase of the occupied bulk states. A nontrivial Zak phase of the occupied bulk states is a dipole moment that leads to edge states. These edge states appear as a projection of the dipole vector on edges, e.g. along x-direction. Besides, if the bulk states have a nontrivial dipole moment in another direction, e.g. along y-direction, these two nonequivalent dipole moments form a quadrupole moment. Then corner states appear as a double projection of quadrupole tensor on corners. On the other hand, the emergence of corner states can also be regarded as a projection of the dipole vector of the occupied edge states. As these edge states inherit the topological properties of the bulk states and corners can be considered as “edges” of edges. This hierarchical picture naturally leads to the following definition of quadrupole moment tensor as [1]

$$Q_{xy} = P_x P_y, \quad (\text{S1})$$

where P_x and P_y are dipole moments along x- and y- directions, respectively. The relation of dipole moment P_i along i -direction (i can be either x or y) and Zak phase, θ_i^{Zak} , is given as [2]

$$P_i = \frac{\theta_i^{\text{Zak}}}{2\pi} = \frac{1}{2\pi} \int_p \langle \psi | i \partial_{k_i} | \psi \rangle \quad (\text{S2})$$

where the integration is along a straight path in i -direction that connects two equivalent k points in 1st Brillouin zone, and ψ is the periodic parts of Bloch functions. In our case, for calculating θ_i^{Zak} , we used the profile of magnetic field component vertical to the slab at each point of the momentum space. A 2D Zak phase, $\theta^{\text{Zak}} = (\theta_x^{\text{Zak}}, \theta_y^{\text{Zak}})$, can be deduced from respective calculations of θ_i^{Zak} for x and y directions.

In general cases, dipole moments are not quantized. However, when the inversion symmetry (C_2 point group symmetry in 2D systems) is present, P_i becomes quantized and can only be either 0 or $\frac{1}{2}$. This quantization is related to a topologically protected winding number of sewing matrix of the occupied bulk states associated with the inversion symmetry. By applying group theory, one finds that the quantization value of dipole moments is solely determined by the parities of the occupied bulk states at high symmetric k points in 1st Brillouin zone, which is given as [3]

$$P_i = \frac{1}{2} \left(\sum_n q_i^n \text{ modulo } 2 \right), \quad (-1)^{q_i^n} = \frac{\eta_n(X_i)}{\eta_n(\Gamma)}, \quad (\text{S3})$$

where the summation is taken over all the energy bands below the band gap, X_i indicates either X or Y points in 1st Brillouin zone, and $\eta_n(\mathbf{k})$ is the parity of the n -th energy band at k point. According to Eqs. (S1) and (S3), we see that if the occupied bulk state has opposite parities at Γ and X (Y) points, nontrivial dipole and quadrupole moments form, together with the emergences of topological edge and corner states in finite samples.

For the designed photonic crystal, it has C_{4v} point group symmetry, which is suitable for applying Eq. (S3). As displayed in Figs. 1(e) to (g) of the main text, the lowest photonic band in the designed photonic crystal can possess opposite parities at Γ and X (Y) points by tuning the air hole size d_2 . Through tuning d_2 , a band inversion happens at $d_1=d_2$, where d_1 is another air hole size in the designed photonic crystal. For $d_2 < d_1$, inverted band structure (the lowest photonic band) that has opposite parities at Γ and X (Y) points forms and so that nontrivial topological dipole and quadrupole moments of bulk states. This nontrivial topological quadrupole moment induces the topological corner states observed in the main text. The band inversion can also occur by shifting the center of unit cell by half a period in the uniform PhC, which corresponds to simply exchanging the hole sizes between d_1 and d_2 .

2. Simulating spectral responses around the corner

We computed the spectral responses plotted in Fig. 3(a) in the main text by using the 2D finite difference time domain (FDTD) method. For the corner spectrum, we allocated the refractive index distribution for the corner made of topologically-distinct PhCs as in Fig. 3(b). The simulation domain was terminated by perfectly matched layers. We put a few current sources at the locations with low spatial symmetry, ensuring the excitation of all the possible modes around the corner. The current sources with lengths of the simulation grid functioned as point dipole radiators. In the time domain, each dipole source emitted an impulse, which equals to while light in the spectral domain. Then, we recorded free evolutions of electromagnetic components at various locations around the corner with low spatial symmetry. The total number of the simulation steps was 32,768, where the time step was set slightly below the stability limit of the simulator. To obtain spectra, we performed Fourier transformation on the recorded time responses. The spectrum for the corner in Fig. 3(a) was of the y -component of electric field (E_y) recorded at $(x, y) = (14.1a, 0.1a)$, where the tip of the corner was taken as the origin of the coordinate. For the spectra of the bulk and 1D edge, we simply replaced the dielectric object to those corresponded in the same simulator and followed the same procedure.

3. Numerical analysis on the device used for the experimental characterization

The PhCs used for the experiment were designed with either $d_1 = 0.6a$ or $0.7a$, while keeping $d_2 = 0$. In the 3D simulations, the lattice constant, a , was set to 335 nm for the case of $d_1 = 0.6a$ and to 375 nm for $d_1 = 0.7a$. The slab thickness was 180 nm. The computed mode distributions are very similar with that presented in Fig. 3(b) in the main text. Using the 3D FDTD method, we computed Q factors of 16,000 for $d_1 = 0.6a$ and 1,800 for $d_1 = 0.7a$. Experimentally, we measured a Q factor of $\sim 2,500$ for $d_1 = 0.6a$ (see the main text) and 600 for $d_1 = 0.7a$. The resonant wavelength of the corner mode was computed to be 1110 nm (1090 nm) for $d_1 = 0.6a$ ($0.7a$). The frequency separation between the corner mode

and the edge of the 1D waveguide modes was calculated by the 3D FDTD method with a similar procedure taken for simulating the spectral response at the corner presented in the previous section. The computed separation of 24 meV (41 meV) for the PhC designed with d_1 of $0.6a$ ($0.7a$) was well comparable with that measured, 21 meV (38 meV).

4. Calculating eigenspectra for topological photonic crystals with corners

For better understanding of the behavior of the PhC investigated in this study, we computed eigenspectra of the topological PhCs covered with trivial PhCs. We considered the same PhC in the main text designed with $d_1 = 0.7a$ and $d_2 = 0.1a$. The PhC was patterned into a square shape with a size of $9a \times 9a$ and was terminated with the corresponding trivial PhC. The total area of the simulation was $18a \times 18a$. To simulate eigenmodes in this structure, we used the 2D plane wave expansion method (i.e. forced periodic boundary conditions). Figure S1 shows a computed distribution of eigenvalues plotted as a function of eigenmode number. A frequency gap is observable between the frequencies of $0.33a/\lambda$ and $0.36a/\lambda$, which reasonably coincide with the mode gap discussed in the main text. Within the gap, there are four eigenstates around a frequency of $0.343a/\lambda$. As expected, they originate from stationary modes localized around the corner. The slight energy dispersion observable in the four states arises from the mutual coupling of the four topological corner states, due to the finite size of the PhC.

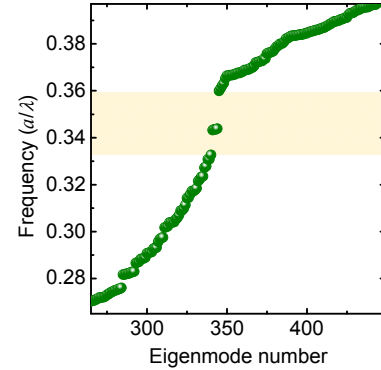


Fig. S1. Calculated eigenmode spectrum.

References

1. F. Liu, H.-Y. Deng and K. Wakabayashi, Phys. Rev. Lett. 122, 086804 (2019).
2. J. Zak, Phys. Rev. Lett. 62, 2747 (1989).
3. C. Fang, M. J. Gilbert, and B. A. Bernevig, Phys. Rev. B 86, 115112 (2012).